Calculation of kaon semileptonic form factor with the PACS10 configuration

Takeshi Yamazaki,^{a,b,*} **Ken-ichi Ishikawa,**^{c} **Naruhito Ishizuka,**^{b}
Yoshinobu Kuramashi,^{b} **Yoshifumi Nakamura,**^{d} **Yusuke Namekawa,**^{e}
Yusuke Taniguchi,^{b} **Naoya Ukita**^{b} **and Tomoteru Yoshié**^{b}

(PACS Collaboration)

^{a}*Faculty of Pure and Applied Sciences, University of Tsukuba, Tsukuba, Ibaraki 305-8571, Japan*

^{b}*Center for Computational Sciences, University of Tsukuba, Tsukuba, Ibaraki 305-8577, Japan*

^{c}*Core of Research for the Energetic Universe, Graduate School of Advanced Science and Engineering,
Hiroshima University, Higashi-Hiroshima, 739-8526, Japan*

^{d}*RIKEN Center for Computational Science, Kobe, Hyogo 650-0047, Japan*

^{e}*Yukawa Institute for Theoretical Physics, Kyoto University, Kyoto 606-8502, Japan*

E-mail: yamazaki@het.ph.tsukuba.ac.jp

We present preliminary results for the kaon semileptonic form factors using the PACS10 configurations, whose physical volume is more than $(10\,\mathrm{fm})^3$ at the physical point with the lattice spacings of 0.085 and 0.064 fm. The configurations were generated using the Iwasaki gauge action and $N_f = 2 + 1$ stout-smeared Clover quark action. For the continuum extrapolation, we calculate the form factors with the local and conserved vector currents. The form factors in the two lattice spacings are extrapolated to the continuum limit using a fit function based on the NLO SU(3) ChPT formula with terms corresponding to finite lattice spacing effects. The value of $|V_{us}|$ is determined using our preliminary result of the form factor at the zero momentum transfer in the continuum limit. The result is compared with recent lattice results, and also predictions of the standard model from the unitarity of the Cabibbo-Kobayashi-Maskawa (CKM) matrix.

---

*Speaker

1. Introduction

One of urgent tasks for the particle physics is to search for signals of physics beyond the standard model. $|V_{us}|$, which is one of the CKM matrix elements, is a candidate of the signal, because recently it was reported [1] that there is a deviation of $|V_{us}|$ between the experimental values determined from the kaon decays, especially the semileptonic (K_{l3}) decay, and an estimation with the unitarity condition of the CKM matrix.

For a precise determination of $|V_{us}|$ through the K_{l3} decay process, it is important to calculate the K_{l3} form factor at the zero momentum transfer squared, $q^2 = 0$, in lattice QCD calculation, because other quantities for $|V_{us}|$ are already determined in the experiment accurately [2]. So far several lattice calculations for the K_{l3} form factor [1, 3–11] were carried out. In this work, for a precise measurement of the form factor and to confirm the deviation of $|V_{us}|$, we perform the calculation using the PACS10 configurations, whose spatial extent is more than 10 fm at the physical point. Using the configuration, finite volume effects are considered to be negligible, and the chiral extrapolation of the form factor is not necessary. Thus, the configuration is suitable for precise measurements of the physical quantities. The results with the PACS10 configuration at the lattice spacing $a = 0.085$ fm were already reported in Ref. [12]. In this report we will show updated results with another PACS10 configuration of $a = 0.064$ fm. All the results presented in this report are preliminary.

2. Simulation parameters

For the generation of the PACS10 configurations, we employ the Iwasaki gauge action [13] and the six stout-smeared Clover quark action in the $N_f = 2 + 1$ QCD. The masses for the light and strange quarks are tuned to be the physical ones. In addition to the ensemble at $a = 0.085$ fm [14] used in our previous calculation [12], another ensemble at $a = 0.064$ fm is used in this work. The parameters for both ensembles are tabulated in Table 1.

The calculation method of the K_{l3} form factors is basically the same in both the lattice spacings, where we evaluate the pion and kaon two-point functions and the K_{l3} three-point function, and extract appropriate matrix elements for the form factors. Details of the method are explained in Ref. [14] for the $a = 0.085$ fm case. At $a = 0.064$ fm, we adopt the hopping parameters for the light and strange quarks, $(\kappa_l, \kappa_s) = (0.125814, 0.124925)$, and the improved Clover coefficient $c_{SW} = 1.02$, which is non-perturbatively determined. We calculate the correlation functions with the $Z(2) \otimes Z(2)$ random source [15]. An exponential smeared source with the random source is also employed at $a = 0.064$ fm to investigate the source dependence of the result. We calculate the three-point functions with several temporal source and sink separations from 3.1 to 4.1 fm for the random source, and from 2.3 to 3.5 fm for the exponential smeared source, respectively. In order to take the continuum limit, the point splitting conserved vector current is employed for the K_{l3} three-point function as well as the local vector current in the two lattice spacings. The statistical error in the calculation is evaluated by the jackknife method.

Table 1: Simulation parameters of the PACS10 configurations in the two lattice spacings. The bare coupling (β), lattice size ($L^3 \cdot T$), physical spatial extent (L[fm]), pion and kaon masses (M_π, M_K) are tabulated. N_{conf} and N_{meas} represent the number of the configurations and the maximum number of the measurement, respectively.

β	$L^3 \cdot T$	L[fm]	a[fm]	M_π[MeV]	M_K[MeV]	N_{conf}	N_{meas}
1.82	128^4	10.9	0.085	135	497	20	1280
2.00	160^4	10.2	0.064	137	501	20	1280

3. Results

3.1 K_{l3} form factors at $a = 0.064$ fm

In this subsection we present preliminary results of the K_{l3} form factors at $a = 0.064$ fm. The matrix element for the K_{l3} form factors given by

$$\langle \pi(p)|V_\mu|K(0)\rangle = (p_K + p_\pi)_\mu f_+(q^2) + (p_K - p_\pi)_\mu f_-(q^2), \tag{1}$$

where $q^2 = -(M_K - E_\pi)^2 + \vec{p}^2$, is extracted from the three-point functions using a proper fit form including excited state effects for π and K as described in Ref. [12]. The temporal wrapping around effects for the mesons are suppressed by averaging the three-point functions with the periodic and anti-periodic boundary conditions in the temporal direction [12]. Since the results from the random and exponential smeared sources are in good agreement with each other, we carry out a combined fit analysis using both the data to extract the matrix elements.

Using the extracted matrix elements, the two form factors, $f_+(q^2)$ and $f_0(q^2)$, are obtained by solving linear equations of Eq. (1) at each q^2. The definition of $f_0(q^2)$ is given by

$$f_0(q^2) = f_+(q^2) - \frac{q^2}{M_K^2 - M_\pi^2} f_-(q^2). \tag{2}$$

The two form factors coincide at $q^2 = 0$, $f_+(0) = f_0(0)$, by the definition.

The preliminary results for $f_+(q^2)$ and $f_0(q^2)$ with the local and conserved currents are presented in Fig. 1 as a function of q^2. Thanks to the large spatial extent in our calculation, we obtain the form factors in a tiny q^2 region with the periodic boundary condition in the spatial directions. The value of $f_+(0)$, which is an essential quantity to determine $|V_{us}|$, is obtained by an interpolation of the form factors to $q^2 = 0$.

We perform the interpolation for each current data independently in Fig. 1. The dashed curves in the figure represent simultaneous fit results using the data for $f_+(q^2)$ and $f_0(q^2)$. As in our previous work [12], the NLO SU(3) ChPT formulas [16, 17] are employed in each form factor given by

$$f_+(q^2) = 1 - \frac{4}{F_0^2}L_9 q^2 + K_+(q^2) + c_0 + c_2^+ q^4, \tag{3}$$

$$f_0(q^2) = 1 - \frac{8}{F_0^2}L_5 q^2 + K_0(q^2) + c_0 + c_2^0 q^4, \tag{4}$$
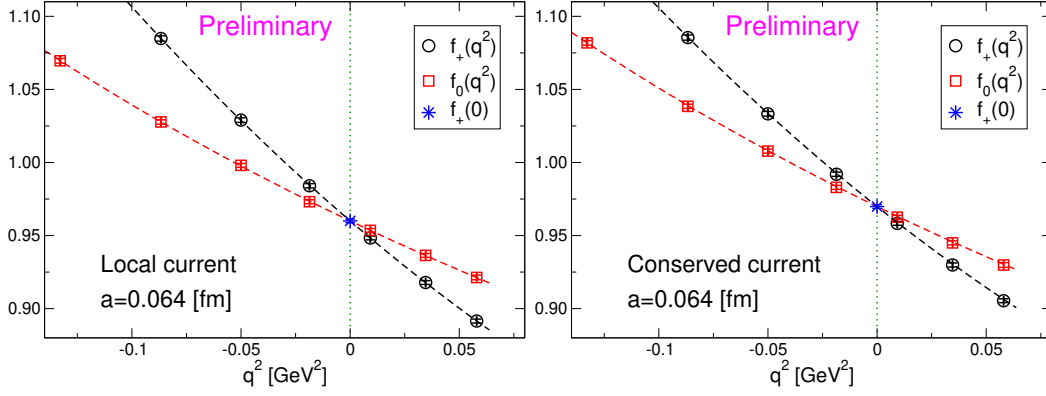
Figure 1: The K_{l3} form factors at $a = 0.064$ fm with the local (left) and conserved (right) currents as a function of q^2. The circle and square symbols represent the data for $f_+(q^2)$ and $f_0(q^2)$, respectively. The dashed curves express their interpolations to $q^2 = 0$ using the fit functions based on the NLO SU(3) ChPT formulas in Eqs. (3) and (4). The fit result of $f_+(0)$ is also plotted by the star symbol.

where L_9, L_5, c_0, and $c_2^{+,0}$ are free parameters. The last two terms in the equations correspond to a part of the NNLO analytic terms. A common c_0 is adopted in the two fit forms to incorporate the constraint at $q^2 = 0$, $f_+(0) = f_0(0)$. The pion decay constant in the chiral limit is fixed to $F_0 = 0.11205$ GeV as in our previous calculation. The two functions $K_+(q^2)$ and $K_0(q^2)$ depend on M_π and M_K, whose explicit forms are shown in Ref. [12]. The simultaneous fits work well in both the current data. The result of $f_+(0)$ is expressed by the star symbol in the figure. While it is hard to see in the figure, we observe a clear difference of the value of $f_+(0)$ with the local and conserved currents. This difference stems from a finite lattice spacing effect, and can be used for the continuum extrapolation of $f_+(0)$.

3.2 Continuum extrapolation of form factors
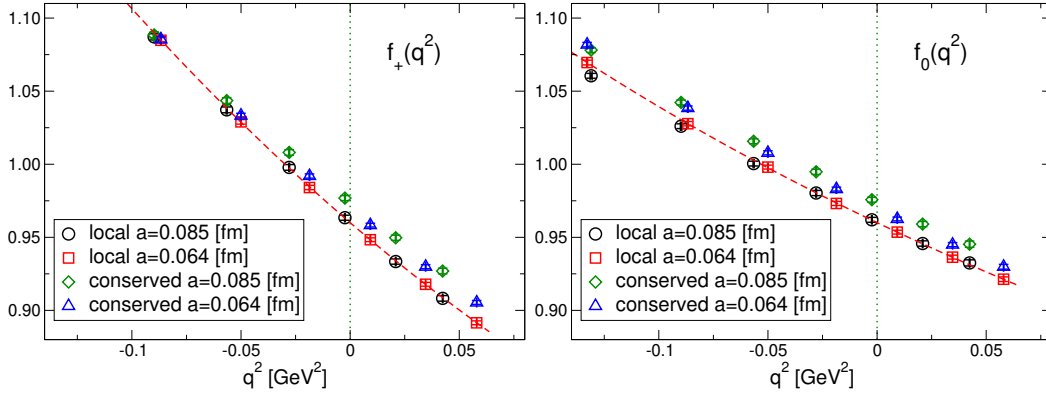
Figure 2: All the data for the K_{l3} form factors, $f_+(q^2)$ (left) and $f_0(q^2)$ (right), in our calculation as a function of q^2. The circle and square denote the local current data at $a = 0.085$ and 0.064 fm, respectively. The diamond and triangle express those for the conserved current data. The dashed curve, which is the fit results of the local current data at $a = 0.064$ fm, is also plotted for comparison.

Figure 2 presents all the data in our calculation for $f_+(q^2)$ and $f_0(q^2)$ in the two different lattice

spacings with the local and conserved currents. The dashed curve is the fit result at $a = 0.064$ fm using the local current data explained in the last subsection.

The local current data of $f_+(q^2)$ at $a = 0.085$ fm is well consistent with the dashed curve in all the q^2 region. It suggests that a finite lattice spacing effect is small in $f_+(q^2)$ with the local current. While the difference between the local and conserved current data increases with q^2 at each lattice spacing, the conserved current data approach to the dashed curve as the lattice spacing decreases.

The lattice spacing dependence of $f_0(q^2)$ is more complicated than the one in $f_+(q^2)$. Nevertheless, the discrepancy between the local and conserved current data decreases with the lattice spacing in all the q^2 region. In the large q^2 region, all the data converge the dashed curve obtained from the local current data. In contrast to the large q^2, the data in the small q^2 region seem to approach the conserved current data as the lattice spacing decreases.
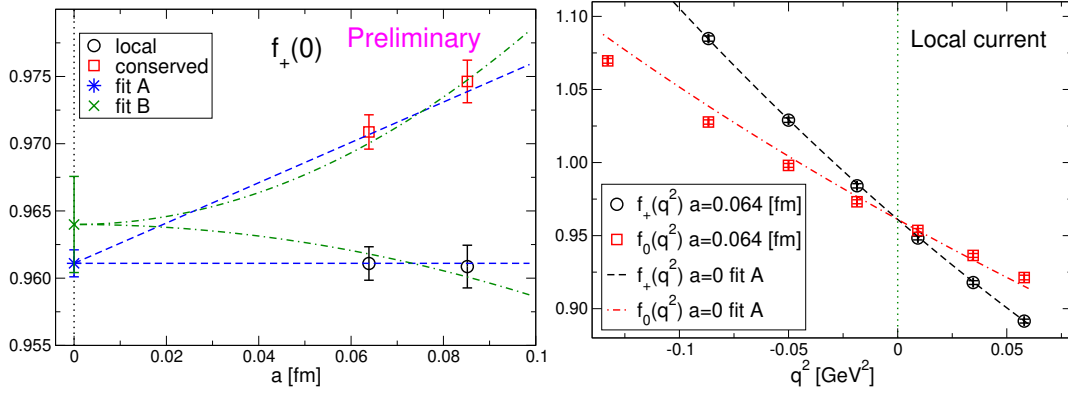
Figure 3: Left: The lattice spacing dependence of $f_+(0)$ with the local (circle) and conserved (square) current data. The continuum extrapolations and the results in the continuum limit with the fit A and B in Eqs. (5)–(8) are also plotted. Right: The continuum results of the fit A for $f_+(q^2)$ and $f_0(q^2)$ are represented by the dashed and dot-dashed curves, respectively, as a function of q^2. The local current data at $a = 0.064$ fm are also plotted for comparison.

The left panel of Fig. 3 shows the results of $f_+(0)$ obtained from the fits based on the NLO SU(3) ChPT formulas in Eqs. (3) and (4) in each lattice spacing with the local and conserved currents as a function of the lattice spacing. While the local current results are reasonably flat against the lattice spacing, the conserved ones show a clear dependence on the lattice spacing.

We carry out simultaneous continuum extrapolations with all the data we obtained. The fitting forms are based on the NLO SU(3) ChPT formulas in Eqs. (3) and (4), and we add terms corresponding to finite lattice spacing effects, which depend on the local and conserved currents as given by

$$f_+^{\mathrm{cur}}(q^2) \;=\; 1 - \frac{4}{F_0^2}L_9 q^2 + K_+(q^2) + c_0 + c_2^+ q^4 + g_+^{\mathrm{cur}}(q^2, a), \qquad (5)$$

$$f_0^{\mathrm{cur}}(q^2) \;=\; 1 - \frac{8}{F_0^2}L_5 q^2 + K_0(q^2) + c_0 + c_2^0 q^4 + g_0^{\mathrm{cur}}(q^2, a), \qquad (6)$$

where cur = loc, con correspond to the local and conserved currents, respectively.

5

From the above observations of the lattice spacing dependence for the form factors, we empirically choose the functions $g_{+,0}^{\rm cur}(q^2, a)$ given as

$$g_+^{\rm loc}(q^2) = 0, \quad g_0^{\rm loc}(q^2) = d_1^0 a^2 q^2, \tag{7}$$

$$g_+^{\rm con}(q^2) = e_0 a + e_1^+ a q^2, \quad g_0^{\rm con}(q^2) = e_0 a + e_1^0 a q^2, \tag{8}$$

where d_1^0, e_0, $e_1^{+,0}$ are free parameters. We shall call this fit as "fit A" in the following. In this choice, we assume that the conserved current data have $O(a)$ errors, which is expected from the lattice spacing dependence of $f_+(0)$ shown in the left panel of Fig. 3. From the fit we obtain the result of $f_+(0)$ denoted by the star symbol in the panel, whose fit lines are expressed by the dashed lines. The fit results for the form factors in the continuum limit as a function of q^2 are plotted in the right panel in the figure together with the local current data at $a = 0.064$ fm for comparison. As discussed in Fig. 2, the fit result of $f_0(q^2)$ is slightly different from the data at $a = 0.064$ fm. In the continuum limit results, we use the experimental values for M_π and M_K instead of their measured values.

In order to estimate systematic error coming from a choice of the fitting form of the continuum extrapolation, we carry out another fit, where we choose the functions $g_{+,0}^{\rm cur}(q^2, a)$ as

$$g_+^{\rm loc}(q^2) = d_0 a^2, \quad g_0^{\rm loc}(q^2) = d_0 a^2 + d_1^0 a^2 q^2, \tag{9}$$

$$g_+^{\rm con}(q^2) = e_0 a^2 + e_1^+ a^2 q^2, \quad g_0^{\rm con}(q^2) = e_0 a^2 + e_1^0 a^2 q^2, \tag{10}$$

with free parameters, d_0, d_1^0, e_0, and $e_1^{+,0}$. This choice is called as "fit B". The reason of this choice is that our improved coefficient $c_{\rm SW}$ is non-perturbatively determined, so that it is simply considered that finite lattice spacing effects start from $O(a^2)$. The fit result of $f_+(0)$ is drawn by the dot-dashed curves in the left panel of Fig. 3. This fit result in the continuum limit denoted by the cross symbol agrees with the one from the fit A, albeit it has larger error.

3.3 Result in the continuum limit

The result of $f_+(0)$ in the continuum limit is plotted in the left panel of Fig. 4. Its central value and the statistical error are determined from the fit A. The systematic error is estimated from the difference of the results for the fit A and B. The preliminary result in this calculation is consistent with that in our previous calculation [12], which is obtained from only the local current data at $a = 0.085$ fm plotted by the open circle in the figure. In this calculation the statistical and systematic errors are improved compared with the previous ones. Our result is roughly consistent with other lattice results in $N_f = 2$ and 2+1 QCD [3–7, 9, 11], while it is slightly smaller than those in $N_f = 2 + 1 + 1$ QCD [1, 8, 10]. At present the reasons are not clear, and we would need detail investigations for the difference in future.

Using the experimental value $|V_{us}| f_+(0) = 0.21654(41)$ [2], we determine the value of $|V_{us}|$ with our preliminary result, which is plotted in the right panel of Fig. 4. The total error contains the statistical and systematic errors in our calculation and also the error from the experiment. For comparison, results from other groups are also plotted in the figure. Our result agrees with the value of $|V_{us}|$ determined from the kaon leptonic (K_{l2}) decay process through $|V_{us}|/|V_{ud}| \times F_K/F_\pi = 0.27599(38)$ [18] using the value of F_K/F_π in PDG18 [18]. We also observe a consistency of
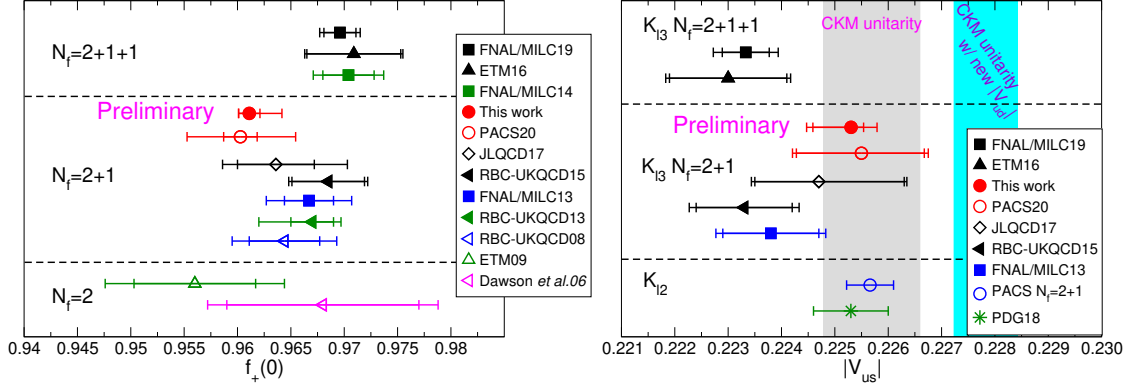
Figure 4: Left: Our preliminary result of $f_+(0)$ in the continuum limit is plotted by the closed circle, together with the result in our previous calculation [12] and those obtained by other groups [1, 3–11]. The closed and open symbols denote results in the continuum limit and at one lattice spacing, respectively. The inner and outer errors express the statistical and total errors. The total error is evaluated by adding the statistical and systematic errors in quadrature. Right: Result of $|V_{us}|$. The symbols are the same in the left panel except for the values from the K_{l2} decay process. Those are determined with F_K/F_π in PDG18 [18] (star) and from the PACS10 configuration at $a = 0.085$ fm [19]. The gray and light blue bands express the values estimated through the unitarity condition of the CKM matrix using the traditional value of $|V_{ud}|$ [18, 20] and the updated one [21], respectively. The inner and outer errors express the lattice and total errors. The total error is evaluated by adding the lattice and experimental errors in quadrature.

our result with the one using the result of F_K/F_π calculated with the PACS10 configuration at $a = 0.085$ fm [19].

Our preliminary result is also in good agreement with $|V_{us}|$ estimated from the unitarity condition of the first row of the CKM matrix using the value of $|V_{ud}|$ in Refs. [18, 20], $|V_{us}| = \sqrt{1 - |V_{ud}|^2}$ where $|V_{ub}|$ is neglected due to $|V_{ub}| \ll |V_{ud}|$. On the other hand, when we use the updated value of $|V_{ud}|$ [21], a clear difference is seen between our preliminary result and the estimated value from the unitarity expressed by the light blue band in the right panel of Fig. 4. This might be a signal of new physics beyond the standard model, while it needs to be investigated with a more precise result.

4. Summary

We have calculated the K_{l3} form factors with the PACS10 configurations at $a = 0.064$ and 0.085 fm. In addition to the local current calculation as in our previous work, the conserved current is employed in the calculation in order to carry out the continuum extrapolation of the form factors. For the continuum extrapolation, simultaneous fits are performed with all the data for the form factors using the fit forms based on the NLO SU(3) ChPT formulas with terms for finite lattice spacing effects.

Our preliminary result of $f_+(0)$ in the continuum limit agrees with our previous work at $a = 0.085$ fm. Our result also reasonably agree with other lattice results except for those in $N_f = 2 + 1 + 1$ QCD, which are little larger than our value. We would need to investigate reasons of the difference in future. Using our preliminary result of $f_+(0)$, the value of $|V_{us}|$ is determined. As

in our previous calculation, it is consistent with the values obtained through the K_{l2} decay, although there is a deviation from the estimated value with the CKM unitarity using the updated $|V_{ud}|$.

In this study we have estimated a systematic error coming from only the continuum extrapolation, so that other systematic errors need to be estimated. Furthermore, since the continuum extrapolation is performed with the data in only two different lattice spacings, at least another lattice spacing data is necessary for a more reliable result in the continuum limit. Towards this direction, we are generating the third PACS10 configuration at a finer lattice spacing.

Acknowledgments

References

[1] **Fermilab Lattice, MILC**, A. Bazavov et al., *Phys. Rev.* **D99** (2019), no. 11 114509, [arXiv:1809.02827].

[2] M. Moulson, *PoS* **CKM2016** (2017) 033, [arXiv:1704.04104].

[3] C. Dawson, T. Izubuchi, T. Kaneko, S. Sasaki, and A. Soni, *Phys. Rev.* **D74** (2006) 114502, [hep-ph/0607162].

[4] **RBC-UKQCD**, P. A. Boyle, A. Juttner, R. D. Kenway, C. T. Sachrajda, S. Sasaki, A. Soni, R. J. Tweedie, and J. M. Zanotti, *Phys. Rev. Lett.* **100** (2008) 141601, [arXiv:0710.5136].

[5] **ETM**, V. Lubicz, F. Mescia, S. Simula, and C. Tarantino, *Phys. Rev.* **D80** (2009) 111502, [arXiv:0906.4728].

[6] **Fermilab Lattice, MILC**, A. Bazavov et al., *Phys. Rev.* **D87** (2013) 073012, [arXiv:1212.4993].

[7] **RBC-UKQCD**, P. A. Boyle, J. M. Flynn, N. Garron, A. Jüttner, C. T. Sachrajda, K. Sivalingam, and J. M. Zanotti, *JHEP* **08** (2013) 132, [arXiv:1305.7217].

[8] **Fermilab Lattice, MILC**, A. Bazavov et al., *Phys. Rev. Lett.* **112** (2014), no. 11 112001, [arXiv:1312.1228].

---

[1]http://luscher.web.cern.ch/luscher/openQCD/

[9] **RBC-UKQCD**, P. A. Boyle et al., *JHEP* **06** (2015) 164, [`arXiv:1504.01692`].

[10] **ETM**, N. Carrasco, P. Lami, V. Lubicz, L. Riggio, S. Simula, and C. Tarantino, *Phys. Rev.* **D93** (2016), no. 11 114512, [`arXiv:1602.04113`].

[11] **JLQCD**, S. Aoki, G. Cossu, X. Feng, H. Fukaya, S. Hashimoto, T. Kaneko, J. Noaki, and T. Onogi, *Phys. Rev.* **D96** (2017), no. 3 034501, [`arXiv:1705.00884`].

[12] **PACS**, J. Kakazu, K.-i. Ishikawa, N. Ishizuka, Y. Kuramashi, Y. Nakamura, Y. Namekawa, Y. Taniguchi, N. Ukita, T. Yamazaki, and T. Yoshié, *Phys. Rev. D* **101** (2020), no. 9 094504, [`arXiv:1912.13127`].

[13] Y. Iwasaki, [`arXiv:1111.7054`]. UTHEP-118.

[14] **PACS**, K. I. Ishikawa, N. Ishizuka, Y. Kuramashi, Y. Nakamura, Y. Namekawa, E. Shintani, Y. Taniguchi, N. Ukita, T. Yamazaki, and T. Yoshié, *Phys. Rev. D* **100** (2019), no. 9 094502, [`arXiv:1907.10846`].

[15] **RBC-UKQCD**, P. A. Boyle, J. M. Flynn, A. Juttner, C. Kelly, H. P. de Lima, C. M. Maynard, C. T. Sachrajda, and J. M. Zanotti, *JHEP* **07** (2008) 112, [`arXiv:0804.3971`].

[16] J. Gasser and H. Leutwyler, *Nucl. Phys.* **B250** (1985) 465–516.

[17] J. Gasser and H. Leutwyler, *Nucl. Phys.* **B250** (1985) 517–538.

[18] **Particle Data Group**, M. Tanabashi et al., *Phys. Rev.* **D98** (2018), no. 3 030001.

[19] **PACS**, K. I. Ishikawa, N. Ishizuka, Y. Kuramashi, Y. Nakamura, Y. Namekawa, Y. Taniguchi, N. Ukita, T. Yamazaki, and T. Yoshie, *Phys. Rev. D* **99** (2019), no. 1 014504, [`arXiv:1807.06237`].

[20] W. J. Marciano and A. Sirlin, *Phys. Rev. Lett.* **96** (2006) 032002, [`hep-ph/0510099`].

[21] C.-Y. Seng, M. Gorchtein, H. H. Patel, and M. J. Ramsey-Musolf, *Phys. Rev. Lett.* **121** (2018), no. 24 241804, [`arXiv:1807.10197`].

PoS(LATTICE2021)563